Journal of *Marine Science and Engineering*

MDPI

Article

Satellite-Based Analysis of Surface Upwelling in the Sea Adjacent to Zhoushan Islands in China

Teng Xiao [1,2], Wenbin Yin [2,*], Jiajun Feng [1], Yingying Liu [1], Kapo Wong [3], Jin Yeu Tsou [4] and Yuanzhi Zhang [1,5]

1 School of Marine Sciences, Nanjing University of Information Science and Technology, Nanjing 210044, China
2 College of Marine Science and Technology, Zhejiang Ocean University, Zhoushan 316022, China
3 Centre for Smart Health, School of Nursing, The Hong Kong Polytechnic University, Hong Kong 999666, China
4 Department of Architecture and Civil Engineering, Faculty of Engineering, City University of Hong Kong, Hong Kong 999666, China
5 Department of Geography and Resource Management, Faculty of Social Science, Chinese University of Hong Kong, Hong Kong 999777, China
* Correspondence: yinwenbin@zjou.edu.cn

Abstract: The fish catch in natural upwelling areas, which accounts for only 0.1% of the ocean surface, accounts for more than 40% of the world's catch. The Zhoushan fishery, which is the largest fishery in China, is mainly formed by a coastal upwelling that features a low temperature. The upwelling in the study area (29.5–31.5° N, 121.5–123.5° E) is a vital factor affecting the formation of the Zhoushan fishery, and the primary productivity and low temperature that are brought by the rising water are important features of the upwelling. This study used global real-time high-resolution multivariate fused satellite (OSTIA) daily sea surface temperature (SST) data developed by the United Kingdom Meteorological Office that were collected from 1981 to 2020 to explore the spatial and temporal variation of the characteristics of the upwelling phenomenon in the study area. The data were processed by a temperature gradient-based upwelling edge detection algorithm to extract information on the central location of the upwelling, the location clusters in the core area, and the intensity index. The quantities of center and core area clusters were counted for each pixel point, and their corresponding probability values were calculated. The results of the spatial and temporal variation of the characteristics of the upwelling show that the upwelling in the study area was generated in April of each year, increased in intensity, and peaked in August, furthermore, the southern part of the upwelling dissipated in September. The region's upwelling is spatially oblique and elliptical, with its long axis following the northeast and extending as far as the mouth of the Yangtze River. Its central location and core area were relatively stably existing in Ma'an Archipelago and Zhongjieshan Islands, which was consistent with the location of the two marine pastures in Zhoushan. According to our findings, locations with higher probability values in the upwelling center and core area, where upwelling occurs frequently, are usually accompanied by higher productivity and offer the potential to develop fishing grounds. The insights that were drawn from the study observations can, therefore, provide some reference for future artificial upwelling site selection.

Keywords: upwelling; Zhoushan islands; SST; probability distribution

Citation: Xiao, T.; Feng, J.; Liu, Y.; Wong, K.; Tsou, J.Y.; Zhang, Y. Satellite-Based Analysis of Surface Upwelling in the Sea Adjacent to Zhoushan Islands in China. *J. Mar. Sci. Eng.* **2023**, *11*, 511. https://doi.org/10.3390/jmse11030511

Academic Editor: José F. Lopes

Received: 27 December 2022
Revised: 13 February 2023
Accepted: 24 February 2023
Published: 26 February 2023

1. Introduction

It is well known that upwelling is the upward movement of seawater below the surface. Upwelling is a phenomenon that is slow-moving in the vertical direction typically characterized by a velocity of only 10^{-6}–10^{-4} m s^{-1} that plays a crucial role in the ocean habitat [1]. The primarily vertical direction of upwelling makes it an essential channel for the exchange of shallow and deep seawater. In particular, upwelling brings nutrients from the depths of the sea to the euphotic zone, conveying high productivity throughout the

whole food chain. Therefore, many areas with upwelling are used as fishing grounds, such as the marine areas near Peru and Zhoushan. Upwelling zones are some of the richest areas in the world and are known for their thriving fishing industry, for example, the United States (West Coast), Angola, etc. [2]. The fish catch in natural upwelling areas, which accounts for only 0.1% of the ocean surface, accounts for more than 40% of the world's catch [3]. The total catch of marine fish accounts for 75% of the total catch, of which about one third are pelagic fish. The most important pelagic fisheries are located in the upwelling zones of the eastern boundary current [4].

Zhoushan has also attracted much attention because of its unique geographical location and the well-known upwelling in the waters there. Subsequent studies have shown that the upwelling in this region is characterized by seasonal variations in summer and winter, as well as according to other timescales [5,6]. In terms of time, the phenomenon begins in late May, strengthens in June, reaches its peak in July and August, and gradually weakens from September to October [5]. In addition to significant seasonal variability, satellite data reveal interannual [3] and short-period variability [7] in this upwelling. There is some controversy over the changes of upwelling intensity in this sea area. Through model data analysis, Yang et al. [8] found that the intensity of summer upwelling in Zhoushan oscillated in cycles of three and eight years over the past 24 years and had a tendency to weaken. On the contrary, Sun et al.'s study of measured wind speed data led the researchers to report a year-by-year increasing trend in upwelling intensity in the coastal waters of Zhoushan [9].

The existing literature presents varying views on factors that are involved in the formation of the Zhoushan upwelling [1]. Ding [10], drawing from hydrometric data and wind data, was the first to discuss the crucial role that wind plays in the short-period variation in coastal upwelling intensity between June and August each year. Similarly, Pan et al. [11] described wind as an important factor in the oscillation of the position of upwelling along the Zhejiang coast, which is affected by the topographic features of the seafloor offshore Zhejiang and the Taiwan Warm Current. Xu et al. [12] analyzed mixed wind field data and contended that wind is the dominant factor for the formation of summer upwelling in Zhoushan sea areas. From a three-dimensional numerical modeling study, Luo et al. [13] reached the conclusion that wind has a stronger influence on the upper upwelling on the sea surface, while the Taiwan Warm Current has a greater influence on the upwelling below the middle layer. Other studies [14,15] have pointed to the contribution of tides in the formation of upwelling in Zhoushan.

Upwelling can be identified by at least three physical variables: wind, sea surface temperature (SST), and chlorophyll a (Chl-a) [16]. Upwelling is accompanied by the exchange of cold deep water and warm surface water, usually differing in temperature between 2 and 4 °C from the surrounding non-upwelling waters, with an average temperature of about 25–28 °C in the upwelling region [5]. In the Zhoushan sea area, Hu [6] found from the SST data that the average temperature difference between the upwelling area and the non-upwelling area is 1.4 °C. The sea surface temperature (SST) in the upwelling region is, therefore, significantly lower than that of the surrounding area, appearing as a spatially oblique, elliptical-shaped cold-water mass on the sea surface on satellite imagery (Figure 1). Studies [8,12] have adopted SSTs to characterize upwelling because of their response to the spatial and temporal distribution and variability of upwelling. Therefore, it is valid to use sea surface temperature to study upwelling in this paper. Although scholars have frequently studied upwelling in the Zhoushan sea areas, no statistical study has previously examined the structure of the upwelling itself, nor have many smaller-scale (daily) and larger-scale (decades) studies been conducted. This paper reports our analysis of SST data from multivariate fusion satellites in Zhoushan-adjacent waters from 1981 to 2020, with an aim to statistically process the distribution of upwelling characteristics on different timescales through preliminary analysis and exploration.

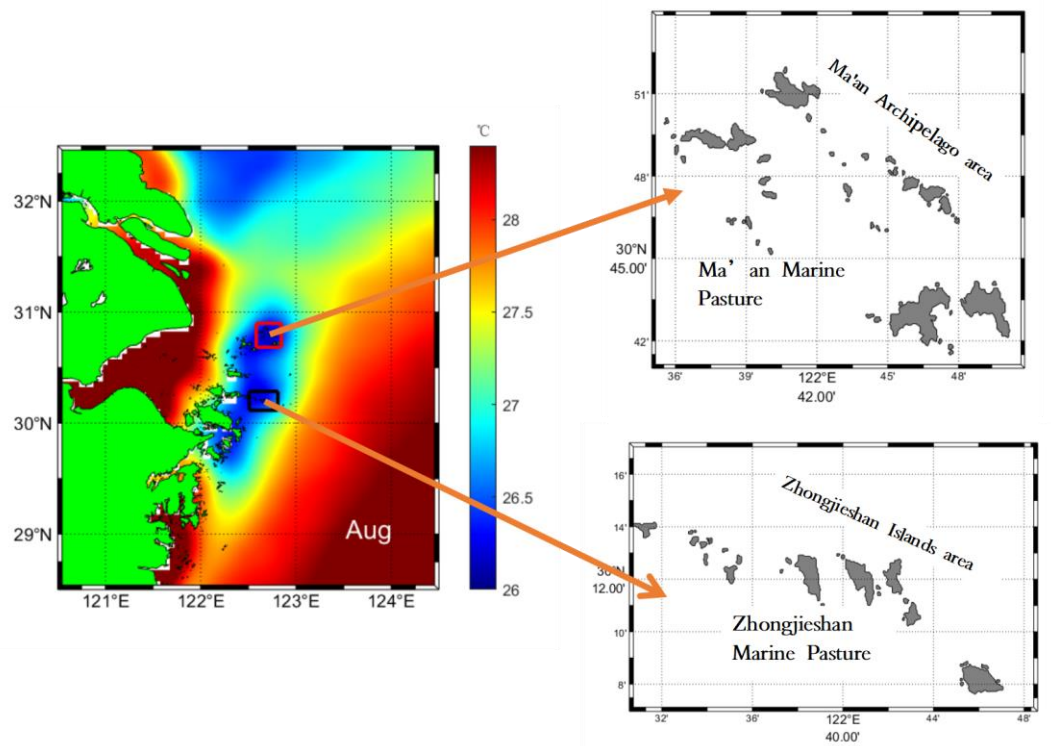

Figure 1. The 40-year average SST in August and two marine pastures.

2. Materials and Methods

2.1. Study Area

This paper's study area is comprised of the sea area adjacent to Zhoushan (29.5–31.5° N, 121.5–123.5° E, Figure 1), located in the shallow waters of the continental shelf in the northwestern part of the East China Sea [7], bordering the Yangtze River Estuary in the north, Hangzhou Bay to the west, and the East China Sea waters in the south. It faces the Pacific Ocean to the east, including the Zhoushan islands, the largest archipelago in China. The areas of focus in the current study are the Ma'an Archipelago and the Zhongjieshan Islands.

2.2. Data

This paper used the global real-time high-resolution multivariate satellite fused daily SST data that were provided by the UK Met Office (UKMO), a time series of nearly 40 years (1981−2020) (download at http://marine.copernicus.eu/, accessed on 31 March 2022) [17], which is used to characterize changes in upwelling characteristics. The data has a time series of 40 years, which can satisfy the study of the differences in upwelling statistical characteristics in the study area. The problem of low data accuracy that is caused by cloud cover and low spatial resolution of microwave remote sensing has been resolved. The fusion product of high resolution of infrared remote sensing and large spatial coverage of microwave remote sensing has been obtained. Through optimal interpolation, infrared remote sensing, microwave remote sensing temperature data from Satellite SST data sources including ESA SST CCI, C3S, EUMETSA and REMSS, and on-site temperature data from HadIOD (drifter and moored buoys) have been fused together. The spatial precision of the data is about 5 km. In the study of upwelling in northeastern Taiwan, Yin [18] compared the UKMO data with the SST data from Himawari-8 (JAXA-SST). The spatial accuracy of JAXA-SST data is about 2 km. The comparison results showed that although the spatial accuracy of UKMO is relatively coarse, it is suitable for the study of upwelling in this area. The range of Zhoushan upwelling is larger than that of northeastern Taiwan, so it is feasible to use UKMO-SST data to study Zhoushan upwelling.

2.3. Methods

2.3.1. Temperature Gradient-Based Edge Detection Algorithm for Upwelling

The research needs of the current study required processing the daily average SST data by using a temperature gradient-based upwelling edge detection algorithm that yielded monthly and multi-year average results. Each result contained the location of the upwelling center, the warm and cold boundary temperature values of the upwelling, the location of the upwelling core, the location of the upwelling sub-center, and the upwelling intensity index (UPI, where the upwelling intensity is the difference between the warm-water boundary temperature and the temperature of the upwelling center) [18].

Upwelling appears as a cold-water mass on the sea surface on satellite images, demonstrating anomalous temperature readings compared with the surrounding area, with the lowest temperature at the center of the upwelling (Four-pointed star C in Figure 2) and a gradual increase in temperature along the radial direction (long black arrow and SST curve in Figure 2) outward to uniformity, while the temperature gradient changes (SST gradient curve in Figure 2). The location of the largest gradient along the radial direction is the cold-water zone boundary (blue line or location b in Figure 2), and the location of the smallest gradient is the warm-water zone boundary (yellow line or location y in Figure 2). The two boundary lines divide the upwelling area into the core area, the mixed zone, and the warm-water area. The temperature of the warm water area and the surrounding sea water is uniform in theory, but there is actually a slight temperature change. In this paper, it can be considered that the warm water area and the surrounding sea water are integrated and do not make a distinction.

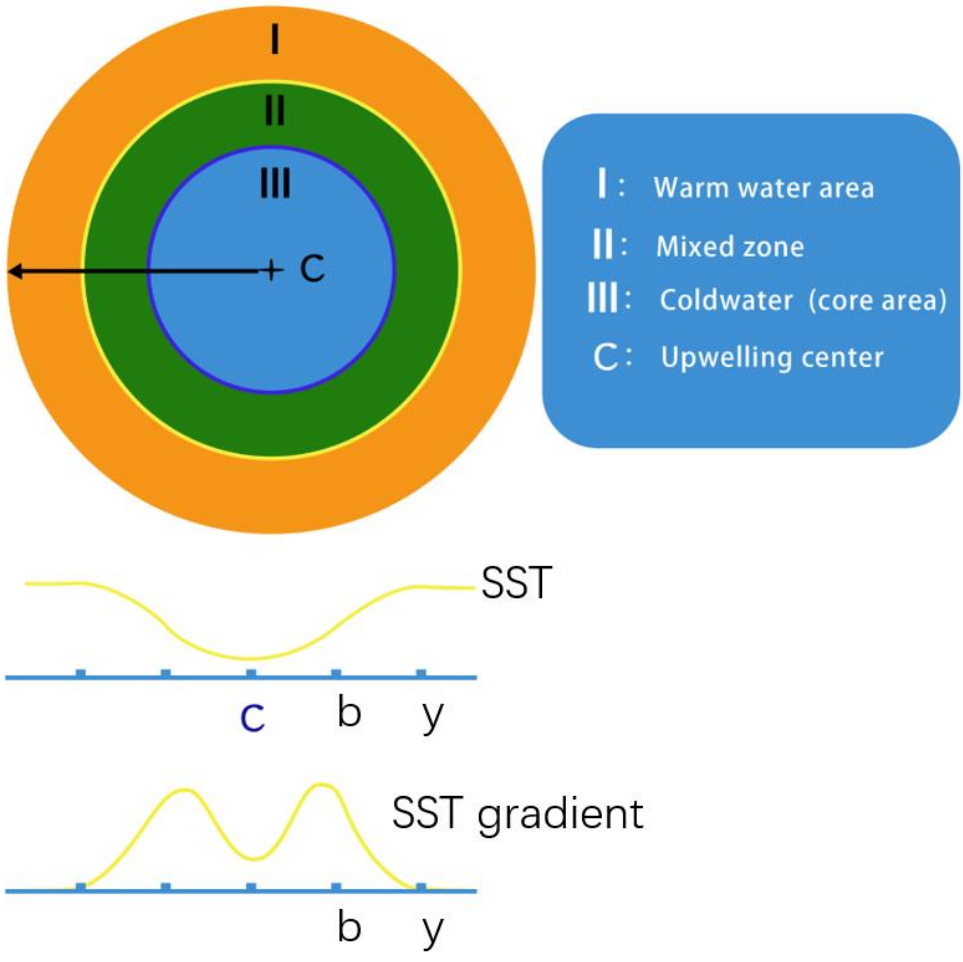

Figure 2. Theoretical sea surface temperature distribution in the upwelling.

From the SST data, several low-temperature locations were captured in descending ranking order, while the lower cryogenic positions of those low-temperature locations were interpreted as the center of the upwelling and the sub-center. The central positions will be used later. A detection circle (consisting of a number of scatter points) was drawn, placing the center of the detection circle at the center of the upwelling. A detection line (radius of the detection circle) was created by connecting the central position of the circle and each circumferential scattered point, interpolating the temperature on the detection line, and performing the above operations on all circumferential scatter points in turn. After obtaining the temperature gradient distribution on all detection lines, the locations where the gradient values were minimal or equal to zero were extracted, and the corresponding temperature value was indexed. Finally, the obtained temperature values were averaged to determine the warm water boundary line temperature values. The boundary line of the core area could also be estimated using the same method [18].

2.3.2. Probability Distribution Calculation Method

There are two main calculations of probability distribution. (1) Central location probability was found by dividing the study area into a grid of pixels at 0.05° each, counting the number of central locations within each pixel grid, and finding the proportion of days when the center of upwelling occurred within a given pixel grid to the total number of days, using the total number of days as a base. (2) The probability distribution of the core area was similar to the central location; the difference was that the core area had multiple locations every day, whereas the central location had only one.

$$UPP(Upwelling\ probability) = \frac{N_{upwellingpoints}}{N_{days}}$$

where $N_{upwellingpoints}$ is the number of times an upwelling center occurs within a pixel grid and N_{days} is the total number of days.

3. Results

3.1. Multi-Year Mean SST Distribution and Variation in Upwelling Intensity

As can be seen from Figure 3, the SST in the study area was evenly distributed from January to March, with little temperature contrast with the surrounding temperature and no significant cold-water mass formation. In April, however, cold-water masses appeared that were cooler than the surrounding seawater in Zhoushan sea. The center of the upwelling only changed at the Ma'an Archipelago and Zhongjieshan Islands from April to August, and the sub-centers were at these two locations and the southeastern part of Zhoushan. In September, the upwelling area began to contract northward and then disappeared from October to December. These observations are in line with the results that were obtained by Huang et al. [19]. From January to March and from October to December, the SST chart shows low-temperature coastal water and high-temperature far-shore water. As we know, there is a large temperature difference between the coast water and the ocean in winter. Furthermore, SST distribution phenomena from January to March and January to December is related to the interaction between the Yangtze River plume and the coastal upwelling. According to research, the existence of rivers can affect the degree of warming in the nearby coastal area [20], which is usually characterized by an increase in the warm season and a decrease in the cold season [21]. This is because the river plume decreases in the warm season, while the river discharge is stronger in winter. Due to the buoyancy of the plume in the Yangtze Estuary, the Ekman transport is enhanced, which enhances the upwelling of the coastal water body, resulting in a lower temperature of the water body. Fernández-Nóvoa also observed this phenomenon in a study on another region [21]. Wu found that the Yangtze River plume has two main paths, one of which is to spread southward along the inshore in winter [22]. In addition, in the study of the world's major

rivers, Fernández-Nóvoa confirmed that the Yangtze River plume will make the nearby coastal area less warm than the ocean [23].

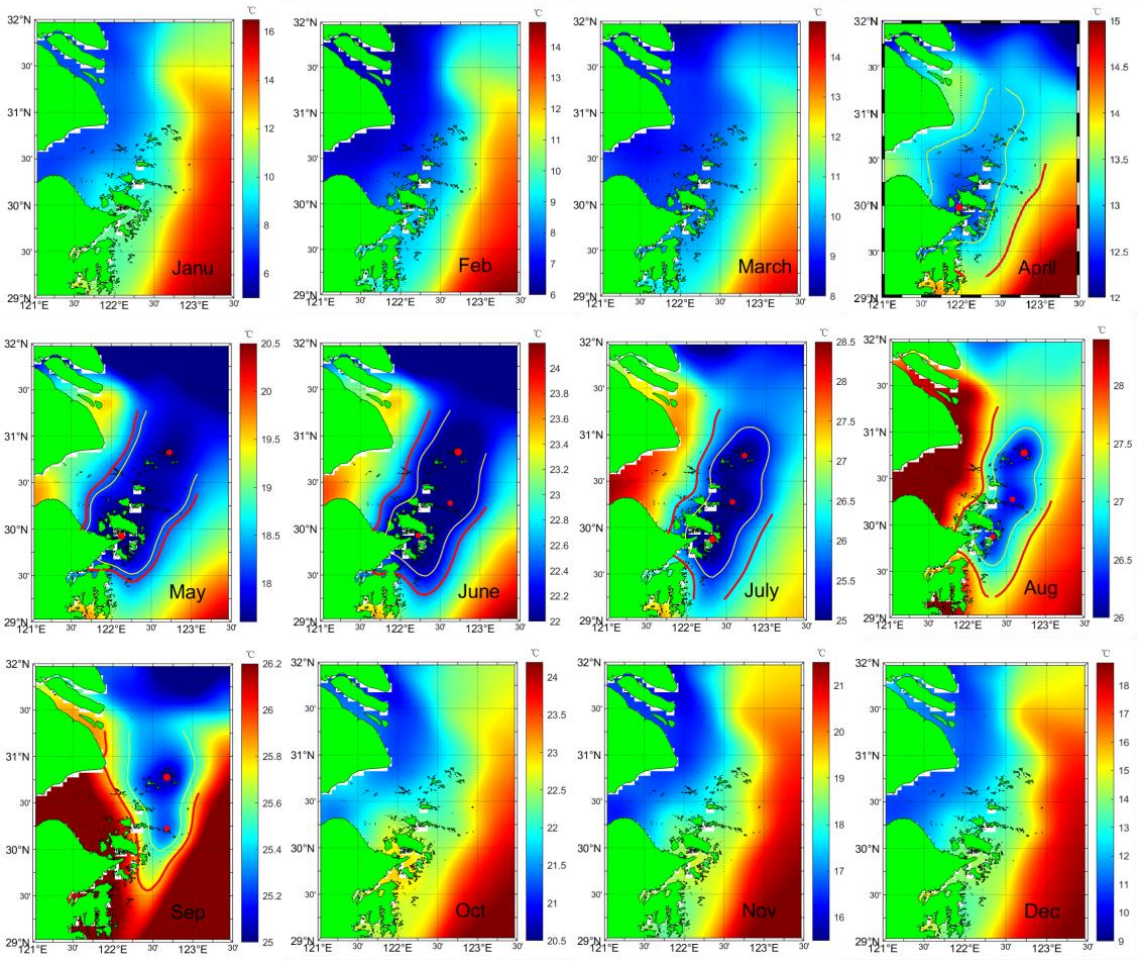

Figure 3. Multi-year average SST distribution (large dots indicate upwelling centers, small dots indicate upwelling sub-centers, yellow lines are core zone boundaries, and red lines are warm water zone boundaries).

To more clearly observe the monthly variation of upwelling intensity for decades and to account for missing data in the initial and final years, the middle three decades (1986–2015) were chosen for the analysis of the five-year intensity changes (Figure 4). It can be seen that the intensity of upwelling in each time period shows roughly the same change, which is the weakest in April, increases continuously from April to August, and weakens from August to September. The average intensity of upwelling is calculated at each stage, and the peak value is in August. The peak values of each stage were 1.5032, 1.7528, 1.6850, 1.5965, 1.7109, and 1.5940 °C, respectively. According to a study on the upwelling in Zhoushan Sea [10], under the influence of the southerly component, the upwelling begins to strengthen in early June, the southerly component strengthens again in late July, and the upwelling strengthens accordingly. This conclusion can be reflected in the intensity change in Figure 5. In addition, the result of Figure 5 complements the change of upwelling intensity from April to June and August to September.

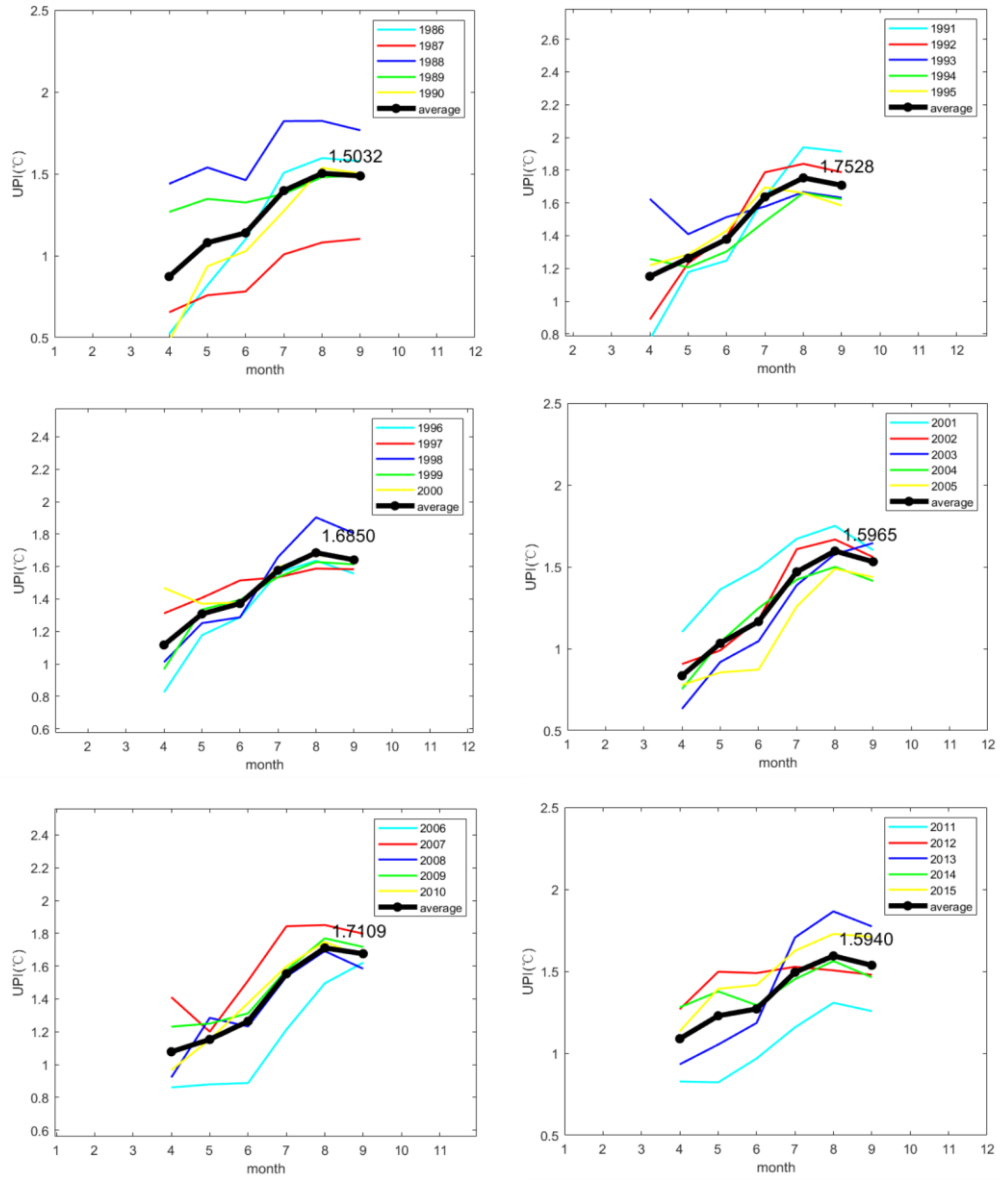

Figure 4. Average monthly intensity of upwelling on a 5-year cycle (from left to right for each phase, 1986–1990, 1991–1995, 1996–2000, 2001–2005, 2006–2010, and 2011–2015).

3.2. Multi-Year Distribution of Centers of Monthy Upwelling from April to September

Figure 5 demonstrates obvious differences in the spatial distribution of the upwelling centers in different months. The centers of upwelling in April were relatively scattered and relatively concentrated in the northern part of the study area, with a small number in the western part of the sea. In May, 13/33 monthly centers were located in the Ma'an Archipelago area. In June, 6/38 and 11/38 monthly centers fell in the Zhongjieshan Islands area and the Ma'an Archipelago area, respectively. There were 13/38 upwelling centers that occurred in the Ma'an Archipelago area in July, and 6 each that occurred in the Zhongjieshan Islands area and southeastern Zhoushan. The number of upwelling center locations in the Ma'an Archipelago area increased to 17 in August, and 7/ 38 upwelling monthly centers still exist in the Zhongjieshan Islands area. A total of 16 out of 36 upwelling centers in the Ma'an Archipelago area and 6/36 centers in the Zhongjieshan Islands area accounted for the total number of upwelling centers in September. By August and September, the centers in the southerly part of the study area had almost disappeared. It can be concluded that from May to September, the Ma'an Archipelago area was always the area where upwelling occurred frequently, and from June to September, although the number of monthly upwelling centers

in the Zhongjieshan Islands area was not as many as that in the Ma'an Archipelago area, it was very stable.

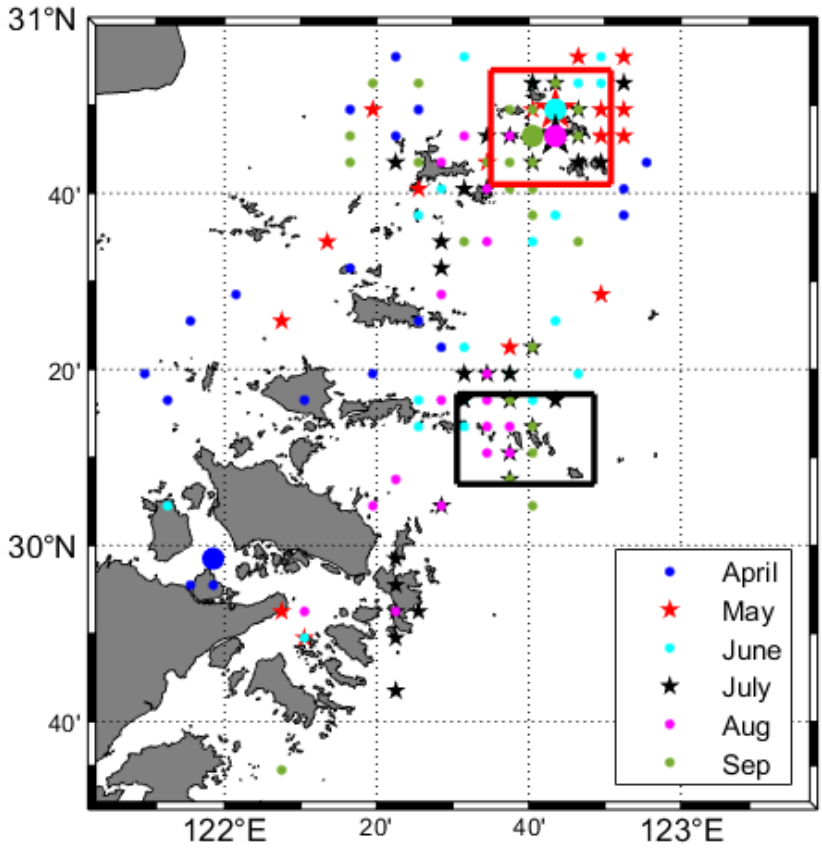

Figure 5. Scatter plot of the location of the centers of upwelling for the same months (April–September) from 1982 to 2020 (large dots are multi-year average centers, small dots are monthly centers. One dot is equal to one-month center.).

3.3. Upwelling Center and Core Area Probabilities

There are three prominent high-probability areas that are presented in Figure 6a, including the area of the Ma'an Archipelago in the north, the Zhongjieshan Islands in the middle, and the southeastern area of Zhoushan. In the probability distribution map of the upwelling core, Figure 6b reveals that these three regions had higher probabilities, which were at 7.0–8.0 $\times$ 10^{-3} in the north, 4.0–6.0 $\times$ 10^{-3} in the middle area, and 3.0–5.0 $\times$ 10^{-3} in the southeast. They were similar in pattern, obliquely elliptical, with the long axis pointing to the northeast and extending to the mouth of the Yangtze River. The core area is distributed around the center of the upwelling. When the upwelling center appears frequently at a certain location, the core area at that location will also appear frequently. Since the spatial distribution of upwelling in the region is mostly present in a diagonal ellipse shape (April–August in Figure 3), this shows the good statistical effect of the 40-year data, and the applicability of this data in presenting the spatial distribution of upwelling in Zhoushan is stable.

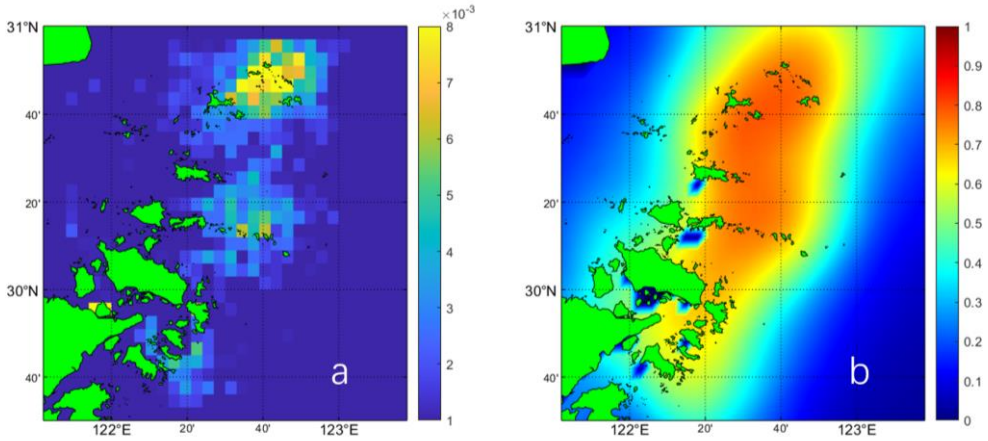

Figure 6. Probability distribution of all April to September daily upwelling centers (**a**) and core areas (**b**), October 1981–June 2020.

In summer (June–August), the upwelling centers were primarily concentrated in the three areas of the Ma'an Archipelago, the Zhongjieshan Islands, and the southern part of Zhoushan. Monthly variations occurred in the central distribution state, scattered from April to May, concentrated from June to August, and relatively scattered in September (compared with the period from June to August). In April, the distribution of upwelling center locations in the study area did not show any obvious aggregation, indicating that the upwelling surge in April was unstable in the satellite data statistics over the past 40 years. From May onward, the distribution of diurnal upwelling center locations gradually became concentrated, and the probability of distribution near the location of the Ma'an Archipelago was relatively high; the probability value of this area was 6.0–8.0 $\times$ 10^{-3}. Another finding was the high value of the probability distribution near the Zhongjieshan area. From June to August, the central location of the upwelling aggregated significantly, with very high values of probability of approximately 7–8 $\times$ 10^{-3} at three locations, two of which were the locations where the marine pasture is located (rectangular box areas in Figure 1). The upwelling was strongest between June and August and occurred around a stable location. By September, the probability value of the south decreased (red box area in Figure 7).

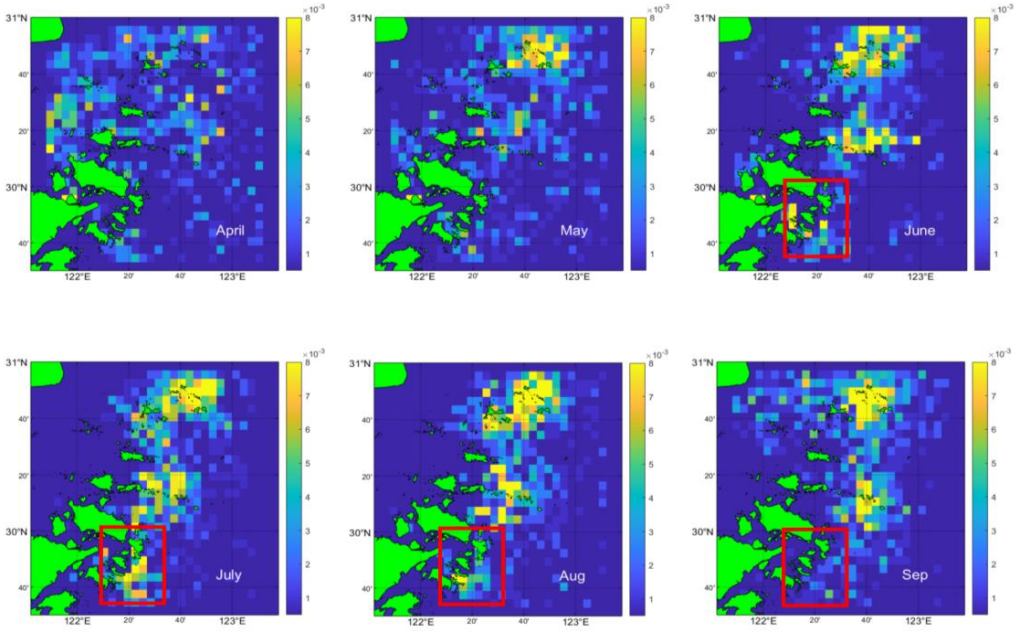

Figure 7. Probability of daily upwelling center location distributions for the same month from 1 October 1981 to 30 June 2020.

The core area of the upwelling in the same month exhibited a spatial pattern distribution that was similar to the location of the center of the upwelling. In April, the number of locations on the same pixel grid was generally lower, and the number of days corresponding to the existence of upwelling was relatively small, which was roughly consistent with the probability distribution of upwelling center locations. In June and August, the probability of the color deepening areas was relatively high, roughly between 0.7 and 0.9. Among them, the probability of core areas in July and August was the highest, concentrated around the Zhongjieshan Islands, the Ma'an Archipelago, and the southeastern part of Zhoushan. By September, the higher probability area in southeastern Zhoushan (black box area in Figure 8) had dissipated. Figure 8 illustrates that the probabilities in the Ma'an Archipelago and Zhongjieshan Islands were still higher in September, which indicates the updraft demonstrated an extended duration.

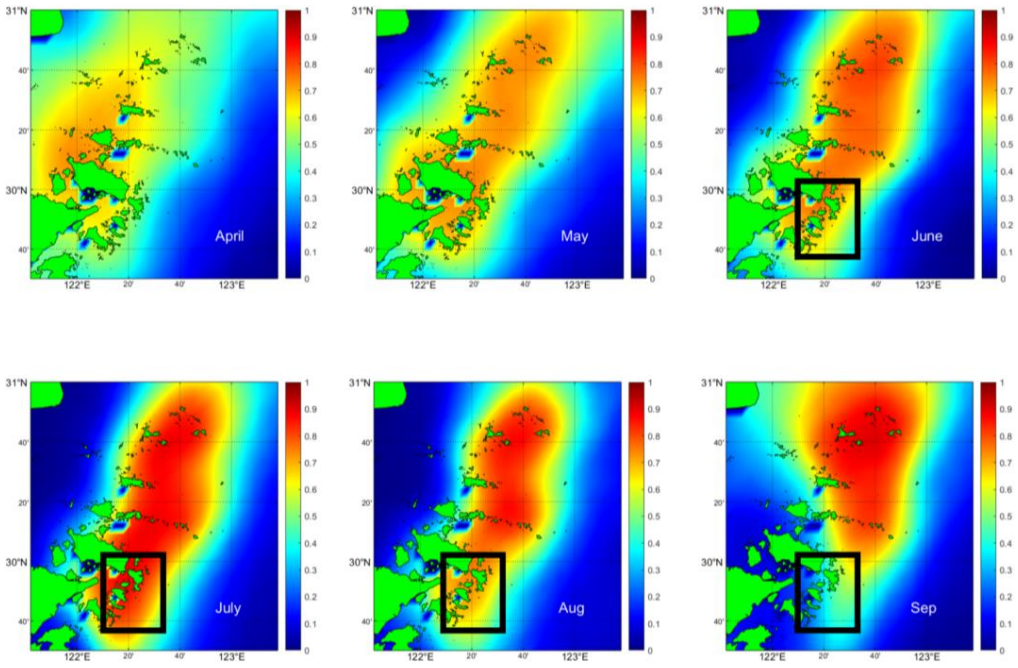

Figure 8. Probability of daily core area of upwelling location distributions for the same month from 1 October 1981 to 30 June 2020.

4. Discussion

4.1. The Role of Seafloor Topography

ETOPO is a type of topographic elevation data. It is published by the U.S. National Geophysical Data Center (NGDC). ETOPO data include ETOPO1, ETOPO2, and ETOPO5 with different accuracy, among which ETOPO1 is the most accurate and recommended. Since ETOPO1 has a fault near 30° N, we chose ETOPO2 data with a spatial accuracy of 60 s for the study. According to our observations, the spatial distribution of the upwelling in the Zhoushan Sea was compatible with the spatial arrangement of the Zhoushan islands, and its boundary line almost wrapped around the entire Zhoushan islands in the form of land close to the edge of Zhoushan. The Zhoushan Sea has an average water depth of 14 m [24] and a long coastline, and the seafloor naturally extends from the land to the sea. It is one of the areas with the widest continental shelf in the world. Hu [7] mentioned that there is a long and narrow slope between the 20 and 50 m contour lines, which is roughly in line with the island. The 30 m isobath is drawn in Figure 9, and it can be seen that the depth lines coincide with the arrangement of the islands. For instance, the trend of the depth line is similar to that of the boundary of the core area in August (Figure 9).

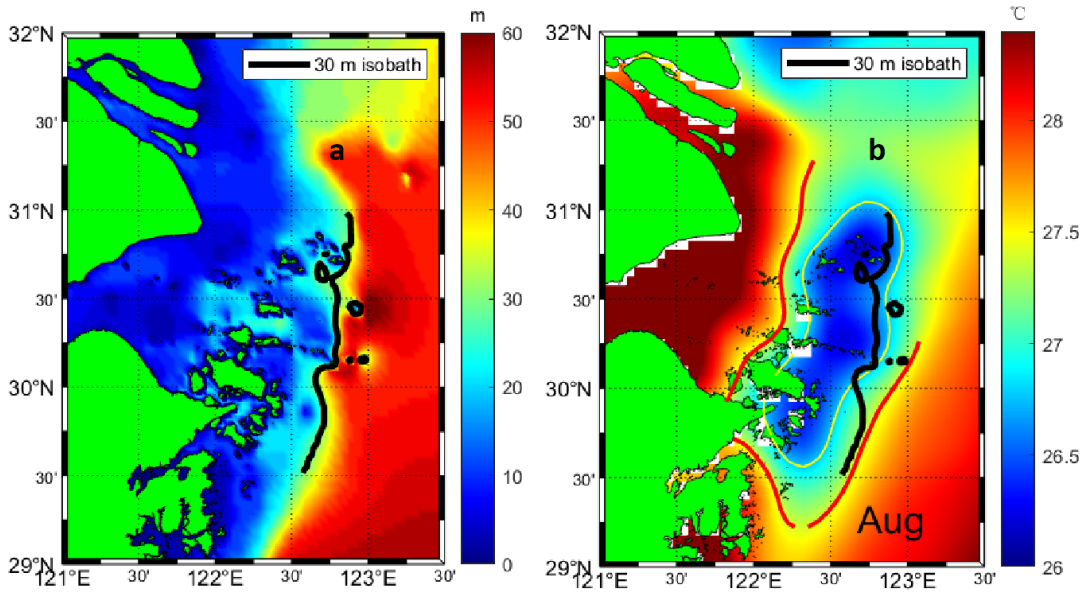

Figure 9. The 30 m isobath in the bathymetry map (**a**) and the SST map (**b**).

4.2. Role of Wind

The influence of wind on upwelling is commonly known as Ekman transport. When the southwest wind blows on the east side of Zhoushan's landform, the southerly wind has a larger component that pushes the surface water body outward, causing deep seawater to replenish upward, thus forming an upwelling. According to Ding [10], around June, the southwest wind prevails in the Zhoushan sea area; thus, the upwelling is gradually stabilized, and there is obviously a strong surge area. From July to August, the southerly wind component increases steadily, leading the upwelling intensity to continue to increase as well. In September, the southerly wind component usually weakens, and the emergence of the southeast wind has a certain hindering effect on the upwelling, causing the spatial distribution in September to demonstrate a V shape.

Upwelling in the Zhoushan waters is a frequently explored research topic. The phenomenon is characterized by significant seasonality; accordingly, most research directions point to seasonality while neglecting the exploration of smaller or larger timescales. This paper employed monthly and decadal analyses of daily data to complement previous studies in terms of timescales. In addition, the study findings present a statistical viewpoint of noteworthy features of upwelling. The study results quantify the frequency of strong upwelling points (centers) and verify the link between national marine pastures and the high-probability area of upwelling centers and core areas. Subsequent research might consider further exploring wind fields and other influencing factors, such as the Warm Taiwan Current, to investigate the Zhoushan regional upwelling from a multidimensional perspective.

4.3. Artificial Upwelling

Artificial upwelling refers to the vertical movement of seawater by engineering means, so as to make up for the limitations of natural upwelling in time and space [4]. The position with a high frequency of natural upwelling can be used as a selection for the site of artificial upwelling. Isaacs et al. [25] proposed to use wave energy to extract deep sea water by changing the density layer distribution of sea water. Liu et al. [26] developed a wave pump artificial upwelling device, which has the advantages of simple structure, low price, reliable performance, and green and sustainable energy, but its flow rate is limited, it cannot reach the nutrient concentration for phytoplankton growth, and it cannot meet the requirements of marine productivity improvement. Aure [27] forcibly lifted the water mass through an electric pump, resulting in an artificial upwelling of nutrient-rich deep water, which greatly increased the primary productivity near the source of the fjord and laid the foundation

for aquaculture. In the exploration and study of Zhoushan area, Yang [3] mentioned that there is a significant vertical temperature and salt stratification at the upwelling position in the Zhoushan area, and because the temperature is negatively related to nutrients, it is meaningful to introduce artificial upwelling at this location.

5. Conclusions

Upwelling in the study area was found to occur in April. At that time, the observed seawater upwelling had no stable area, and its intensity was weak. Between May and August, upwelling developed around a stable central range and continued to increase in intensity, peaking at about 1.5–1.7 °C in August. The probability value in the southern part of the study area was close to zero in September, indicating that the extent of the upwelling shrank in that month, while the southern seawater was no longer vertically exchanged, the surface seawater temperature was low and could not be maintained, and the intensity had a negative growth, which was probably related to the influence of the monsoon shift. Combining the results over the entire 40-year period revealed that the synoptic centers were mainly distributed in the Ma'an Archipelago and the Zhongjieshan Islands, and the monthly mean center positions were consistent with the general trend of synoptic center distribution. In addition, the probabilities of diurnal upwelling centers and the core areas showed similar spatial distribution characteristics, while the areas with higher probability values were located in the Ma'an Archipelago and Zhongjieshan Islands, consistent with the locations of the two marine pastures in Zhoushan. The probability values were about 7.0–8.0 $\times$ 10^{-3} for the Ma'an Archipelago and 0.7–0.8 for the Zhongjieshan Islands. The above results confirm the higher probability values of the upwelling center and core area that are usually associated with higher productivity and easier fishery production. Thus, this study's findings can be expected to provide a certain reference for future artificial upwelling site selection.

Author Contributions: Conceptualization, T.X. and W.Y.; methodology, T.X., W.Y. and J.F.; validation, T.X. and Y.Z.; formal analysis, T.X., Y.Z. and J.F.; investigation, T.X., Y.L. and K.W.; resources, J.Y.T. and Y.Z.; data curation, T.X. and W.Y.; writing—original draft preparation, T.X; writing—review and editing, K.W. and Y.Z.; visualization, J.F., Y.L. and K.W.; supervision, Y.Z.; project administration, Y.L.; funding acquisition, Y.Z.; All authors have read and agreed to the published version of the manuscript.

Funding: This research was funded by the National Natural Science Foundation of China (Grant No. U1901215), the Marine Special Program of Jiangsu Province in China (JSZRHYKJ202007), and the Natural Scientific Foundation of Jiangsu Province (BK20181413).

Institutional Review Board Statement: Not applicable.

Informed Consent Statement: Not applicable.

Data Availability Statement: Data can be available from the Copernicus Marine Environment Monitoring Service (CMEMS, http://marine.copernicus.eu/, accessed on 31 March 2022) for daily SST, and NOAA (https://www.ngdc.noaa.gov/mgg/global/global.html, accessed on 24 January 2023) for depth.

Acknowledgments: Dataset from Copernicus Marine and Environmental Monitoring Service (CMEMS) is highly appreciated. The research was funded by the National Natural Science Foundation of China (U1901215).

Conflicts of Interest: The authors declare no conflict of interest.

References

1. Hu, J.; Wang, X.H. Progress on upwelling studies in the China seas. *Rev. Geophys.* **2016**, *54*, 653–673. [CrossRef]
2. Jayaram, C.; Jose, F. Relative dominance of wind stress curl and Ekman transport on coastal upwelling during summer monsoon in the southeastern Arabian Sea. *Cont. Shelf Res.* **2022**, *244*, 104782. [CrossRef]
3. Yang, J.; Zhang, D.; Chen, Y.; Fan, W.; Liang, H.; Tan, M. Feasibility analysis and trial of air-lift artificial upwelling powered by hybrid energy system. *Ocean. Eng.* **2017**, *129*, 520–528. [CrossRef]

4. Zhu, J.; Huang, H.; Lin, H.; Lei, X.; Zheng, R. Efficient estimation of chlorophyll a concentration in artificial upwelling. *Math. Comput. Simul.* **2021**, *185*, 660–675. [CrossRef]
5. Lou, X.; Shi, A.; Xiao, Q.; Zhang, H. Satellite observation of the Zhejiang coastal upwelling in the East China sea during 2007-2009. *Proc. Spie* **2011**, *8175*, 283–304.
6. Hu, M.N.; Zhao, C.F. Long-time observation of upwelling in the Zhoushan Islands and adjacent seas during the summer season. *Period. Ocean. Univ. China* **2007**, *1*, 235–240.
7. Hu, M.; Zhao, C. Upwelling in Zhejiang coastal areas during summer detected by satellite observations. *J. Remote Sens.* **2008**, *12*, 304.
8. Yang, S.; Mao, X.; Jiang, W. Interannual variation of coastal upwelling in summer in Zhejiang, China. *Period. Ocean. Univ. China* **2020**, *50*, 1–8.
9. Sun, Y.; Dong, C.; He, Y.; Yu, K.; Renault, L.; Ji, J. Seasonal and interannual variability in the wind-driven upwelling along the southern East China sea coast. *IEEE J. Sel. Top. Appl. Earth Obs. Remote Sens.* **2016**, *9*, 5151–5158. [CrossRef]
10. Ding, Z. Influences of wind on vertical structures of temperature and salinity, and upwelling off Zhejiang coast in summer. *Chin. J. Oceanol. Limnol.* **1985**, *3*, 109–117.
11. Pan, Y.; Xu, D.; Xu, J. The front structures, variation and cause of the upwelling front zone off Zhejiang. *Acta Oceanol. Sin.* **1985**, *4*, 401–411.
12. Xu, Q.; Zhang, S.; Cheng, Y.; Zuo, J. Interannual feature of summer upwelling around the Zhoushan Islands in the East China Sea. *J. Coast. Res.* **2017**, *33*, 125–134. [CrossRef]
13. Luo, Y. Numerical studies of wind-and TWC-driven upwelling in coastal areas of the East China Sea. *J. Ocean Univ.* **1998**, *28*, 536–542.
14. Xingang, L.U.; Qiao, F.L.; Xia, C.S.; Yuan, Y.L. Tidally induced upwelling off yangtze river estuary and in zhejiang coastal waters in summer. *Sci. China Earth Sci.* **2007**, *50*, 462–473.
15. Lü, X.; Qiao, F.; Xia, C.; Zhu, J.; Yuan, Y. Upwelling off Yangtze River estuary in summer. *J. Geophys. Res.* **2006**, *111*, A7. [CrossRef]
16. Budiman, A.S.; Bengen, D.G.; Nurjaya, I.W.; Arifin, Z.; Ismail, M.F.A. A comparison of the three upwelling indices in the South Java sea shelf. *CMU J. Nat. Sci.* **2022**, *21*, e2022044. [CrossRef]
17. Stark, J.D.; Donlon, C.J.; Martin, M.J.; McCulloch, M.E. OSTIA: An operational, high resolution, real time, global sea surface temperature analysis system. In Proceedings of the Oceans 2007—Europe, Aberdeen, UK, 18–21 June 2007; IEEE: Piscataway, NJ, USA; pp. 1–4.
18. Yin, W.; Huang, D. Short-term variations in the surface upwelling off northeastern taiwan observed via satellite data. *JGR Oceans* **2019**, *124*, 939–954. [CrossRef]
19. Huang, Q.; Xu, Q.; Zhang, S.; Cheng, Y. Study of coastal upwelling around Zhoushan Islands based on satellite measurements and numerical model. In Proceedings of the 2016 Progress in Electromagnetic Research Symposium (PIERS), Shanghai, China, 8–11 August 2016; pp. 4764–4768.
20. Ffield, A. Amazon and Orinoco River plumes and NBC rings: Bystanders or participants in hurricane events? *J. Clim.* **2007**, *20*, 316–333. [CrossRef]
21. Fernández-Nóvoa, D.; Costoya, X.; Kobashi, D.; Rodríguez-Díaz, L.; deCastro, M.; Gómez-Gesteira, M. Influence of Mississippi and Atchafalaya River plume in the winter coastal cooling of the Northwestern Gulf of Mexico. *J. Mar. Syst.* **2020**, *209*, 103374. [CrossRef]
22. Wu, H.; Shen, J.; Zhu, J.; Zhang, J.; Li, L. Characteristics of the Changjiang plume and its extension along the Jiangsu Coast. *Cont. Shelf Res.* **2014**, *76*, 108–123. [CrossRef]
23. Fernández-Nóvoa, D.; Costoya, X.; DeCastro, M.; Gómez-Gesteira, M. Influence of the mightiest rivers worldwide on coastal sea surface temperature warming. *Sci. Total Environ.* **2021**, *768*, 144915. [CrossRef] [PubMed]
24. Hao, Z.; Chen, L.; Wang, C.; Zou, X.; Zheng, F.; Feng, W.; Zhang, D.; Peng, L. Heavy metal distribution and bioaccumulation ability in marine organisms from coastal regions of Hainan and Zhoushan, China. *Chemosphere* **2019**, *226*, 340–350. [CrossRef]
25. Isaacs, J.D.; Castel, D.; Wick, G.L. Utilization of the energy in ocean waves. *Ocean. Eng.* **1976**, *3*, 175–187. [CrossRef]
26. Liu, C.C.; Jin, Q. Artificial upwelling in regular and random waves. *Ocean. Eng.* **1995**, *22*, 337–350. [CrossRef]
27. Aure, J.; Strand, Ø.; Erga, S.R.; Strohmeier, T. Primary production enhancement by artificial upwelling in a western Norwegian fjord. *Mar. Ecol. Prog. Ser.* **2007**, *352*, 39–52. [CrossRef]